JACS
JOURNAL OF THE AMERICAN CHEMICAL SOCIETY
Article
pubs.acs.org/JACS

Experimentally Quantifying Small-Molecule Bond Activation Using Valence-to-Core X-ray Emission Spectroscopy

Christopher J. Pollock,[†] Katarzyna Grubel,[‡] Patrick L. Holland,[‡] and Serena DeBeer*[,†,§]

[†]Max-Planck-Institut für Chemische Energiekonversion, Stiftstrasse 34-36, D45470 Mülheim an der Ruhr, Germany
[‡]Department of Chemistry, University of Rochester, Rochester, New York 14627, United States
[§]Department of Chemistry and Chemical Biology, Cornell University, Ithaca, New York 14853, United States

Supporting Information

ABSTRACT: This work establishes the ability of valence-to-core X-ray emission spectroscopy (XES) to serve as a direct probe of N_2 bond activation. A systematic series of iron-N_2 complexes has been experimentally investigated and the energy of a valence-to-core XES peak was correlated with N−N bond length and stretching frequency. Computations demonstrate that, in a simple one-electron picture, this peak arises from the N_2 2s2s σ^* orbital, which becomes less antibonding as the N−N bond is weakened and broken. Changes as small as 0.02 Å in the N−N bond length may be distinguished using this approach. The results thus establish valence-to-core XES as an effective probe of small molecule activation, which should have broad applicability in transition-metal mediated catalysis.

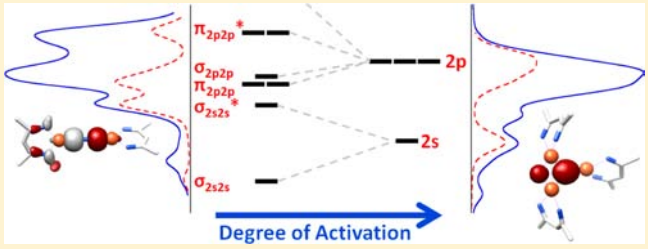

INTRODUCTION

The controlled activation of small molecules by transition metal catalysts is vital to countless chemical, biological, and industrial processes, including N_2 reduction,[1−3] water splitting,[4−6] and hydrocarbon functionalization.[7] Crucial to understanding the mechanisms of these transition metal mediated reactions is the need to experimentally probe the process by which the metal "activates" (i.e., weakens) bonds in a small molecule substrate. The extent of bond activation is traditionally probed using vibrational spectroscopy, but there remain numerous examples where reactive intermediates have eluded characterization by conventional vibrational techniques.[8−11] This may be attributed in part to the selection rules that limit the number of modes with significant intensity in IR and Raman spectra. For example, the N−N stretching modes of centrosymmetric bridging N_2 compounds are not IR active, necessitating Raman spectroscopy of compounds that may not be stable to laser irradiation. For this reason, site selective methods such as nuclear resonance vibrational spectroscopy (NRVS) have had a large impact on the identification of vibrational states in iron complexes.[8,9,12] However, NRVS requires elements with accessible nuclear excited states, limiting its practical applications in catalysis to iron systems.

In the present study, we take a different approach and use valence-to-core X-ray emission spectroscopy (XES) to examine the differences in the electronic structures of Fe−N_2 complexes in order to obtain insight into the degree of N−N bond activation. Though the examples given here focus on iron and the activation of N_2, the strategy should be applicable to any accessible transition metal and to the activation of various small molecules (e.g., O_2, CO_2, CO, H_2O, C_xH_y).

XES is an element specific technique where high energy X-rays generate a 1s core hole on a metal atom and the photons emitted when electrons decay to fill the vacancy are measured (Figure 1).[13,14] The intensity of these spectra is governed by

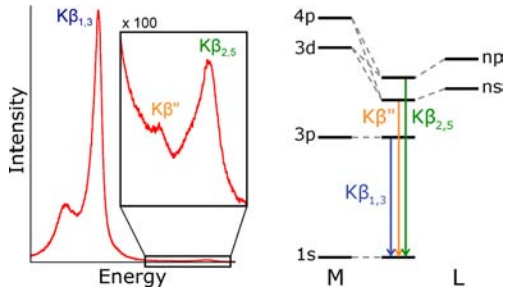

Figure 1. Schematic representation of X-ray emission.

the dipole selection rule, whereby the oscillator strength is modulated by the amount of metal *n*p character present in the donor orbital. Hence, transitions from metal 2p orbitals ($K\alpha$ emission) and 3p orbitals ($K\beta$ emission) are both possible and give intense features. Moreover, any filled ligand-based valence orbitals that possess appreciable metal p character will also display emission features ($K\beta''$ and $K\beta_{2,5}$ "valence-to-core" emission), albeit with relatively low intensity.

This latter region of the spectrum is of particular interest due to its sensitivity to the chemical environment around a metal center. It is known, for instance, that valence-to-core XES is

Received: December 4, 2012
Published: July 17, 2013

   dx.doi.org/10.1021/ja3116247 | J. Am. Chem. Soc. 2013, 135, 11803−11808

sensitive to ligand identity, hybridization, protonation state, and metal–ligand bond length.[14−16] Further, in previous studies, we have shown that the valence-to-core region of the XES spectrum can be interpreted using a simple molecular orbital (MO) based picture and provides a map of any ligand MOs possessing appreciable metal p character.[17] For complexes with simple ligands (e.g., ferrocene or $Fe(CN)_6^{3-}$),[17,18] MO theory can easily be utilized to predict and assign valence-to-core spectra without any computational assistance. This is an important point to stress, because, while the results of density functional theory (DFT) calculated spectra often have excellent agreement to experiment and aid in interpretation, analysis of the XES spectra is not dependent on computational results.

It is for these reasons that XES holds promise as an effective spectroscopic probe of small molecule activation. Given the large energetic changes encountered during bond weakening and the sensitivity of valence-to-core XES to ligand electronic structure, XES should, in principle, provide a direct probe of the extent of ligand bond activation. Here we explore this possibility by investigating a series of iron complexes with bound dinitrogen moieties (Figure 2). All of these complexes

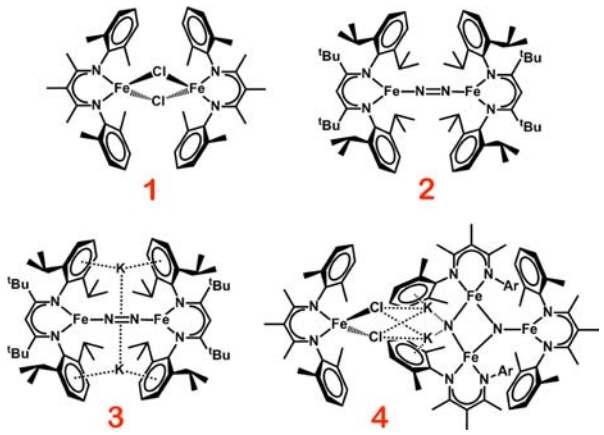

Figure 2. The compounds used in this study display various degrees of N–N bond activation.

utilize β-diketiminate as a supporting ligand, but they achieve varying degrees of N_2 activation that range from a partially activated N–N triple bond in **2**, to a more activated N–N bond in **3**, and a fully cleaved bis-nitride in **4**; compound **1** serves as a control and allows us to assess the contribution of the N-based diketiminate ligand. The experimental valence-to-core XES data are quantitatively assessed in an MO-based picture and further correlated to DFT calculations. Using these data, together with previously published data sets, linear correlations between the energy of an XES peak corresponding to the N_2 2s2s σ^* orbital and the N–N bond length become evident. Hence, the present study demonstrates valence-to-core XES as a novel probe of small-molecule bond activation.

EXPERIMENTAL SECTION

Sample Preparation. The compounds studied here were prepared according to published procedures.[19,20] Because of the extreme air sensitivity of these compounds, all sample preparations and manipulations were conducted in a glovebox under an atmosphere of dry, purified N_2. Samples for X-ray emission analysis were prepared by grinding the solid to a fine powder with boron nitride, packing into a 1 mm aluminum cell, and sealing with 38 μm Kapton tape.

Data Collection and Processing. All XES spectra were collected at SSRL beamline 6–2 (54 pole wiggler, 1 T) with ring current of 350 mA. The incident beam energy was set to 8 keV using a Si(111) liquid nitrogen cooled monochromator and was calibrated using a Fe foil. Focusing mirrors were used to achieve a 140 μm × 400 μm beam at the sample, providing ~10^{13} photons/second. If necessary to prevent sample damage or detector saturation, aluminum filters were inserted before the sample to attenuate the incident beam. Energy resolution of the XES spectrometer was achieved using a crystal array spectrometer employing five spherically bent Ge(620) crystals (100 mm diameter, 1 m radius of curvature) aligned on intersecting Rowland circles.[14] Samples were maintained at <20 K in an Oxford CFI208 continuous flow liquid helium cryostat and were positioned at 45° with respect to the incident beam. A He filled flight path was used between the sample and spectrometer to reduce signal attenuation and emitted X-rays were detected using an energy resolving Si drift detector with a 3 mm vertical slit.

Spectra were collected over the energy range of 7020 to 7130 eV with steps of 0.2 eV (7020–7080 eV) and 0.15 eV (7080–7130 eV). The signal was normalized with respect to the incident flux measured in a He filled ion chamber. The spectrometer energy was calibrated using scans of Fe_2O_3 with reference energies of 7044.22, 7060.71, 7092.38, and 7107.42 eV. Damage was assessed by performing successive scans at the same spot to determine appropriate exposure times. All scans that showed no evidence of damage were averaged using PyMCA,[21] and the area under the entire spectrum was set to 1000. Averaged spectra were fit using BlueprintXAS[22] version 1.2; reported values are the average of at least 30 good fits.

Computations. All calculations were performed using the ORCA version 2.9 quantum chemical suite.[23] Geometry optimizations and XES spectral calculations were performed using the BP86 functional[24,25] and the scalar-relativistically recontracted def2-TZVP basis set.[26] The expanded CP(PPP) basis set[27] was used for Fe along with a special integration accuracy of 7. Starting coordinates for optimizations were obtained from crystal structures.[19,20] Calculated XES spectra were shifted by a constant value of 182.5 eV, based on a previous calibration study.[14] Molecular orbitals were visualized with contour levels of 0.035 using Chimera 1.5.3[28] and deconvolution of the N_2 contribution to the spectra was performed using MOAnalyzer.[29]

RESULTS AND ANALYSIS

To test the ability of XES to monitor small molecule activation, a series of previously reported iron β-diketiminate complexes were investigated (Figure 2).[19,20] As noted above, these compounds use similar supporting ligands to achieve varying degrees of N–N bond activation, including systematic lengthening of the N–N bonds from **2** to **3** and complete N–N bond cleavage in **4**. Thus, these compounds provide an ideal test case for studying the sensitivity of XES to small molecule activation.

XES spectra were collected on all four compounds shown in Figure 2 and an overlay of the valence-to-core region is shown in Figure 3a. These spectra are highly featured and, most importantly, show the appearance of a peak at approximately 7100 eV only for the compounds that contain N_2-derived N (**2**, **3**, and **4**); a feature at roughly this energy previously has been associated with ligated N_2 in bis(imino)pyridine-supported iron-N_2 compounds.[30] From the selection rules governing XES and simple MO considerations, all filled N_2-based orbitals should in principle contribute to the spectra. However, previous work on compounds with the isoelectronic cyanide ligand has revealed that this region of the spectrum is dominated by the 2s2s σ^* orbital of the diatomic, the diffuse nature of which allows for strong interaction with the metal *n*p orbitals;[17] computational evidence to support this assignment and further discussion is presented below (*vide infra*). Notably, the position of this peak shifts to lower energies as the N–N distance is

dx.doi.org/10.1021/ja3116247 | J. Am. Chem. Soc. 2013, 135, 11803–11808

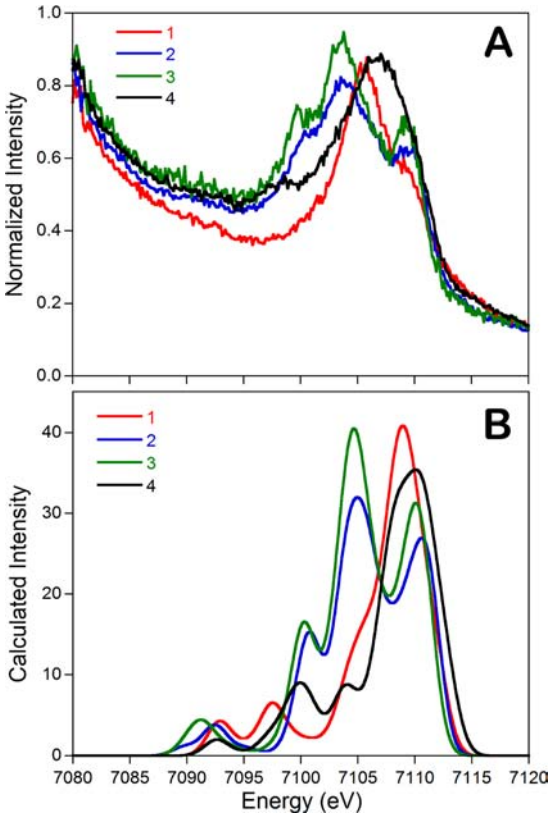

Figure 3. Significant differences in the valence-to-core XES spectra are seen between the investigated compounds, most notably the appearance of a feature around 7100 eV when N_2-derived N is present. The experimental spectra (A) are in good agreement with the calculations (B).

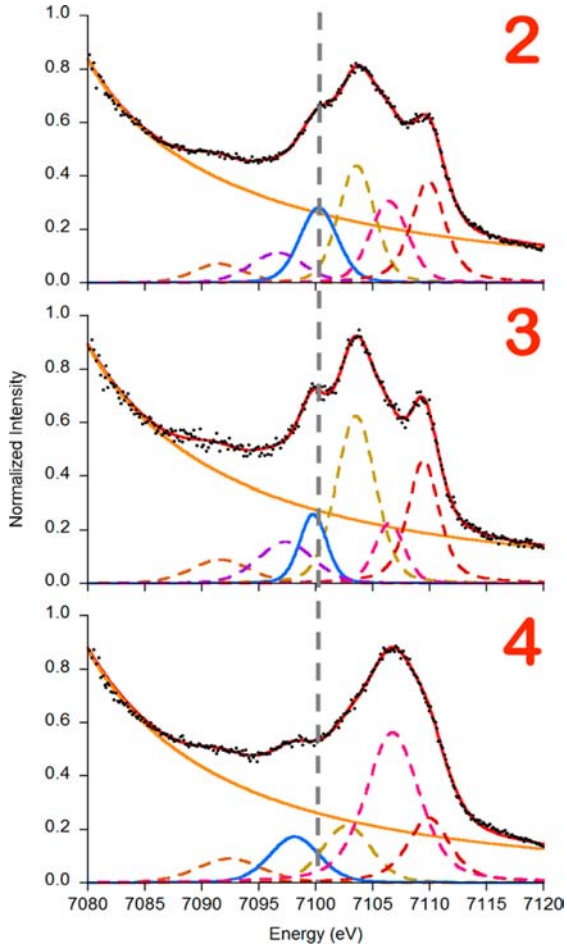

Figure 4. Spectral deconvolutions for compounds **2**, **3**, and **4**. Of greatest interest is the solid blue peak that changes position with N−N bond length. The guideline is centered at 7100.25 eV to allow easier visualization of spectral changes.

Table 1. Bond Lengths, XES Energies, and Vibrational Data for Relevant N_2-Containing Compounds[19,20,30,31]

	N···N distance	XES energy	vibrational frequency
2	1.182 Å	7100.25 eV	1778 cm^{-1}
3	1.232 Å	7099.77 eV	1589 cm^{-1}
4	2.799 Å	7098.14 eV	
(^{iPr}PDI)FeN_2	1.110 Å	7100.56 eV	2046 cm^{-1}
(^{iPr}PDI)$Fe(N_2)_2$	1.097 Å[a]	7100.69 eV	2089 cm^{-1}[a]

[a]The two unique N−N lengths and stretches in this compound were averaged to obtain these values.

lengthened, suggesting sensitivity to the degree of N−N activation.

To better quantify the changes observed, deconvolutions of the spectra were performed using BlueprintXAS[22] (Figure 4, Table 1). The quantitative results demonstrate a dramatic downward shift of 2.1 eV in the peak position as the N−N bond length is increased from slightly activated in **2** to fully cleaved in **4**. Furthermore, comparison to previously characterized compounds[30] that bind but do not activate N_2 demonstrates a linear correlation between the energy position of this putative 2s2s σ^* feature and the N−N bond length (Figure 5a). The energy of this N_2 derived feature also correlates very well with the experimental N−N stretching frequencies, a standard measure for the degree of activation (Figure 5b).[32] This latter point is especially important because it calibrates and validates the utility of XES as a probe of N−N bond length in these systems.

With the correlations to bond length and stretching frequency established, DFT calculations were employed to obtain further insight into the origins of these spectral changes. Geometry optimized structures (see Supporting Information) were used to calculate XES spectra using established methods[14] (Figure 3b). The calculated spectra qualitatively reproduce experiment very well and capture all of the important features present, including the shift to lower energy of the ∼7100 eV peak.

Importantly, the DFT calculations allow insight into the nature of the spectral transitions. The spectra were calculated using a one electron model, so each MO gives rise to a single XES transition, making deconvolution and assignments of the peaks straightforward. This approach has been used previously[15,30] to successfully assign contributions from single atoms and various functional groups. Of greatest importance here is to confirm that the XES feature of interest does indeed derive from the N_2 moiety and that the supporting ligand does not significantly contribute to this peak.

To this end, we have utilized MOAnalyzer to perform a fragment deconvolution of the contributions to these valence-to-core spectra (Figure 5, Supporting Information). This method of deconvolution requires that MOs can be cleanly assigned to a given fragment. In the case of the N_2 fragments, this is straightforward as the MOs of interest are relatively pure

dx.doi.org/10.1021/ja3116247 | J. Am. Chem. Soc. 2013, 135, 11803−11808

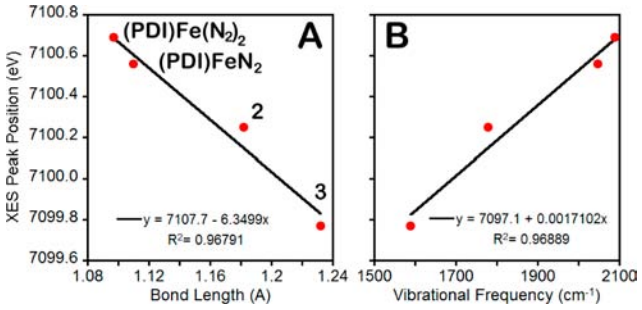

Figure 5. Correlations between the energy of the N_2-derived XES peak and (A) the N−N bond length and (B) the N−N stretching frequency.

and energetically well-separated from the β-diketiminate orbitals. In the case of the β-diketiminate fragment itself, however, the inherently larger number of MOs—particularly at higher energies—makes this more complex, though meaningful assignments may still be made.

To assess the N_2 contribution to the spectrum of **2**, we began by analyzing the Löwdin populations of the orbitals to identify those that derive from the N_2 fragment. Three orbitals immediately stand out in this analysis, labeled a, b, and c in Figure 6, which contain 98%, 94%, and 70% N_2 + Fe character, respectively. Inspection of the contour plots for these enables easy assignment: it is readily apparent that the N_2 2s2s σ bonding and antibonding orbitals give transitions at 7088 and 7100 eV, respectively, while the 2p2p σ orbital can be seen to slightly higher energy at 7103 eV (Figure 6). Further, it is clear that for the 7100 eV transition a large majority (~75%) of the intensity comes from the N_2 2s2s σ^* with minimal contribution from surrounding features.

The intensities of these three transitions—and the absence of any appreciable intensity deriving from the 2p2p π bond—can be rationalized according to the extent with which these orbitals interact with the Fe *n*p orbitals. Both the 2s2s σ^* and 2p2p σ are relatively diffuse with significant electron density directed toward the metal centers in a σ fashion (Figure 6), thus allowing strong mixing with the metal and high intensities. The 2s2s σ bonding orbital also has a σ interaction with the metals, though it is much more localized on the N_2 unit and thus mixes less with the metal *n*p, giving lower intensity. Finally, the 2p2p π orbital is both highly localized on the N_2 and lacks any σ interactions with the metals, giving rise to almost no p mixing and negligible intensity. We note that, should the coordination mode of the N_2 unit change (e.g., from end-on to side-on binding), the orbitals giving rise to intense XES features would also be expected to change,[33−36] though these new peaks would also be sensitive to the N−N bond length in a manner analogous to the trends observed for the present series. For the β-diketiminate ligand, a larger number of ligand-based MOs are involved, which necessarily makes the assignment of individual transitions to specific orbital less direct than in the case of N_2 (see Supporting Information, Figure S1 for a demonstration of this effect using **1**). Nonetheless, the β-diketiminate derived MOs are found at a higher energy than the N_2 MOs and, importantly, the contributions are well separated from the N_2 2s2s σ^* contribution.

Taking the energetic and intensity considerations together, we can see that the analysis of diatomics is a fortunate case in that an intense feature is present in a region of the spectrum that is unobscured by the contributions from most other ligands. This occurs because the strong triple bond between the nitrogens pushes the 2s2s σ^* orbital to high energy, away from the region where many other ligands would contribute. This same reasoning could be applied to other diatomics as well (e.g., CO, O_2, NO), suggesting broad applicability of this technique to assessing small molecule activation.

Thus, with the spectral feature at ~7100 eV assigned as the N_2 2s2s σ^* orbital, the shift to lower energy upon bond lengthening and breaking that is observed can easily be rationalized. As the N_2 unit becomes more activated, the overlap between the orbitals on the two N atoms decreases until, in the extreme case of **4**, all that remains are noninteracting N 2s and 2p orbitals. This decrease in overlap lowers the energy of the 2s2s σ^* orbital until the bond is completely cleaved, resulting in two isolated 2s orbitals, accounting for the observed shift of this feature. These effects are represented graphically in Figure 7. Thus, the computational results are entirely consistent with the view provided by a simple MO-based analysis of the experiment.

CONCLUDING REMARKS

These results demonstrate that the activation of N_2 by an iron complex can be monitored by valence-to-core XES. The 7100

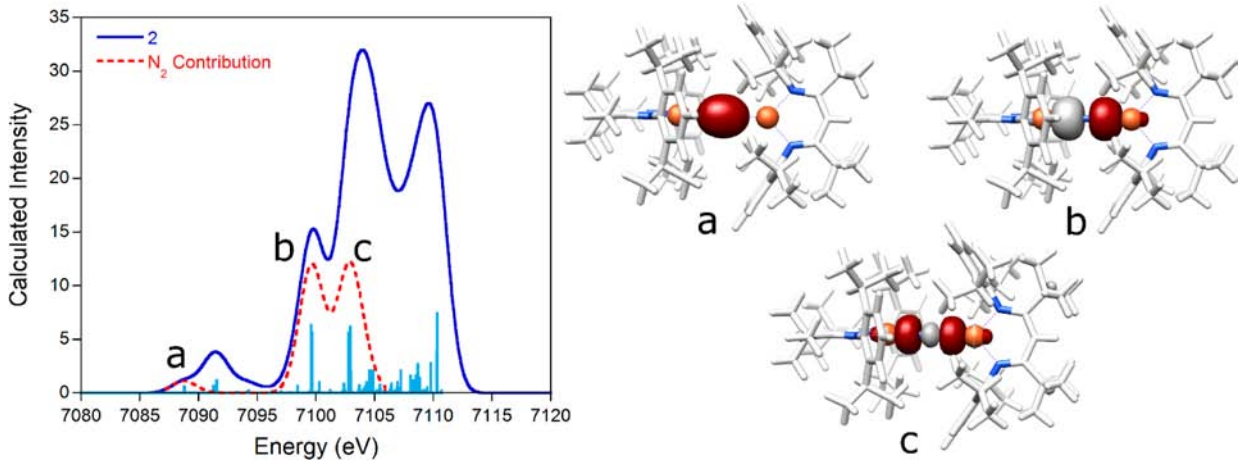

Figure 6. Assignment of the important N_2-derived features from the calculated XES spectrum for **2**. The blue curve is the total calculated spectrum, while the red represents only the contribution from the indicated N_2 orbitals.

dx.doi.org/10.1021/ja3116247 | J. Am. Chem. Soc. 2013, 135, 11803−11808

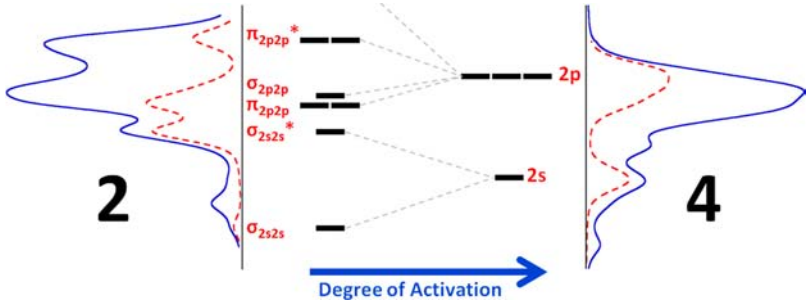

Figure 7. A qualitative MO scheme depicting the origin of the spectral changes observed from compounds **2** to **4**. The total calculated spectrum is shown (blue) along with the deconvoluted N−N contribution (red). Note that while the 2p2p π* orbital is formally empty, there is a significant backbonding interaction with the metal d-orbitals (~30% N character) and so we have included it on this plot to illustrate the collapse of the 2p manifold. As the N−N bond is lengthened, the 2s2s σ* orbital drops in energy until the bond is completely broken and all that remains are two isolated N 2s orbitals. The calculated spectra have been shifted relative to one another to better visualize these effects.

eV feature in **2** can be assigned to the N_2 2s2s σ* orbital on the basis of MO theory arguments and this assignment is further supported by DFT calculations. As the N−N bond is lengthened in **3** by 0.05 Å, this peak shifts 0.5 eV to lower energy, consistent with less destabilization of the antibonding orbital at longer bond lengths. Finally, upon complete cleavage of the N−N bond in **4**, a large shift is observed as now only isolated N 2s orbitals are present.

It thus is apparent that valence-to-core XES can provide a very sensitive probe of small molecule activation, allowing for discrimination of even small bond length changes in complex systems; with an experimental precision of 0.2 eV, differences in bond length as small as 0.02 Å can be detected. This compares favorably with vibrational techniques because, even though the resolution of XES is relatively low, the energy differences between the electronic states being probed are large and thus they may be distinguished by XES. Importantly, the selection rules governing XES dictate that any ligand-based orbital with appreciable metal *n*p mixing can potentially be observed, allowing element specific access to many systems not amenable to vibrational analysis. Further, recent developments in dispersive spectrometers[37−39] increasingly allow XES to be translated into a time-resolved domain, giving it promise as a probe of chemical catalysis in real time.

■ ASSOCIATED CONTENT

Supporting Information

Deconvoluted calculated XES spectrum of **1**, ORCA input files, optimized coordinates. This material is available free of charge via the Internet at http://pubs.acs.org.

■ AUTHOR INFORMATION

Corresponding Author

serena.debeer@cec.mpg.de

Notes

The authors declare no competing financial interest.

■ ACKNOWLEDGMENTS

We thank Vera Krewald for assistance with recalcitrant ORCA optimizations. Financial support was provided by the Alfred P. Sloan foundation, the Max-Planck-Gesellschaft, the Fulbright Foundation, and the US National Institutes of Health (GM-065313). Portions of this research were carried out at the Stanford Synchrotron Radiation Lightsource (SSRL), a national user facility operated by Stanford University on behalf of the US Department of Energy, Office of Basic Energy Sciences.

■ REFERENCES

(1) Ertl, G. *Angew. Chem., Int. Ed.* **2008**, *47*, 3524−3535.
(2) Hoffman, B. M.; Dean, D. R.; Seefeldt, L. C. *Acc. Chem. Res.* **2009**, *42*, 609−619.
(3) Somorjai, G. A. *J. Mol. Struct. (THEOCHEM)* **1998**, *424*, 101−117.
(4) Barber, J. *Chem. Soc. Rev.* **2009**, *38*, 185−196.
(5) Kudo, A.; Miseki, Y. *Chem. Soc. Rev.* **2009**, *38*, 253−278.
(6) Nocera, D. G. *Acc. Chem. Res.* **2012**, *45*, 767−776.
(7) Nam, W. *Acc. Chem. Res.* **2007**, *40*, 522−531.
(8) Liu, L. V.; Bell, C. B.; Wong, S. D.; Wilson, S. A.; Kwak, Y.; Chow, M. S.; Zhao, J.; Hodgson, K. O.; Hedman, B.; Solomon, E. I. *Proc. Natl. Acad. Sci.* **2010**, *107*, 22419−22424.
(9) Petrenko, T.; DeBeer George, S.; Aliaga-Alcalde, N.; Bill, E.; Mienert, B.; Xiao, Y.; Guo, Y.; Sturhahn, W.; Cramer, S. P.; Wieghardt, K.; Neese, F. *J. Am. Chem. Soc.* **2007**, *129*, 11053−11060.
(10) Noguchi, T. *Coord. Chem. Rev.* **2008**, *252*, 336−346.
(11) McEvoy, J. P.; Brudvig, G. W. *Chem. Rev.* **2006**, *106*, 4455−4483.
(12) Paulat, F.; Berto, T. C.; DeBeer George, S.; Goodrich, L.; Praneeth, V. K. K.; Sulok, C. D.; Lehnert, N. *Inorg. Chem.* **2008**, *47*, 11449−11451.
(13) Glatzel, P.; Bergmann, U. *Coord. Chem. Rev.* **2005**, *249*, 65−95.
(14) Lee, N.; Petrenko, T.; Bergmann, U.; Neese, F.; DeBeer, S. *J. Am. Chem. Soc.* **2010**, *132*, 9715−9727.
(15) Delgado-Jaime, M. U.; Dible, B. R.; Chiang, K. P.; Brennessel, W. W.; Bergmann, U.; Holland, P. L.; DeBeer, S. *Inorg. Chem.* **2011**, *50*, 10709−10717.
(16) Beckwith, M. A.; Roemelt, M.; Collomb, M.-N. l.; DuBoc, C.; Weng, T.-C.; Bergmann, U.; Glatzel, P.; Neese, F.; DeBeer, S. *Inorg. Chem.* **2011**, *50*, 8397−8409.
(17) Pollock, C. J.; DeBeer, S. *J. Am. Chem. Soc.* **2011**, *133*, 5594−5601.
(18) Lancaster, K. M.; Finkelstein, K. D.; DeBeer, S. *Inorg. Chem.* **2011**, *50*, 6767−6774.
(19) Smith, J. M.; Sadique, A. R.; Cundari, T. R.; Rodgers, K. R.; Lukat-Rodgers, G.; Lachicotte, R. J.; Flaschenriem, C. J.; Vela, J.; Holland, P. L. *J. Am. Chem. Soc.* **2006**, *128*, 756−769.
(20) Rodriguez, M. M.; Bill, E.; Brennessel, W. W.; Holland, P. L. *Science* **2011**, *334*, 780−783.
(21) Sole, V. A.; Papillon, E.; Cotte, M.; Walter, P.; Susini, J. *Spectroc. Acta Pt. B* **2007**, *62*, 63−68.
(22) Delgado-Jaime, M. U.; Mewis, C. P.; Kennepohl, P. *J. Synchrotron Radiat.* **2010**, *17*, 132−137.
(23) Wennmohs, F.; Becker, U.; Ganyushin, D.; Hansen, A.; Liakos, D. G.; Izsak, R.; Kollmar, C.; Kossmann, S.; Petrenko, T.; Reimann, C.; Riplinger, C.; Römelt, M.; Sandhoefer, B.; Shapiro, I.; Sivalingam, K.; Valeev, E.; Wezisla, B. *ORCA—An ab Initio, Density Functional and Semiempirical Program Package*, version 2.9.0; University of Bonn: Bonn, Germany, 2012.

(24) Perdew, J. P. *Phys. Rev. B* **1986**, *33*, 8822.
(25) Becke, A. D. *Phys. Rev. A* **1988**, *38*, 3098.
(26) Pantazis, D. A.; Chen, X. Y.; Landis, C. R.; Neese, F. *J. Chem. Theory Comput.* **2008**, *4*, 908−919.
(27) Neese, F. *Inorg. Chim. Acta* **2002**, *337C*, 181.
(28) Pettersen, E. F.; Goddard, T. D.; Huang, C. C.; Couch, G. S.; Greenblatt, D. M.; Meng, E. C.; Ferrin, T. E. *J. Comput. Chem.* **2004**, *13*, 1605−1612.
(29) Delgado-Jaime, M. U.; DeBeer, S. *J. Comput. Chem.* **2012**, *33*, 2180−2185.
(30) Stieber, S. C. E.; Milsmann, C.; Hoyt, J. M.; Turner, Z. R.; Finkelstein, K. D.; Wieghardt, K.; DeBeer, S.; Chirik, P. J. *Inorg. Chem.* **2012**, *51*, 3770−3785.
(31) Bart, S. C.; Lobkovsky, E.; Chirik, P. J. *J. Am. Chem. Soc.* **2004**, *126*, 13794−13807.
(32) Holland, P. L. *Dalton Trans.* **2010**, *39*, 5415−5425.
(33) Ohki, Y.; Fryzuk, M. D. *Angew. Chem., Int. Ed.* **2007**, *46*, 3180−3183.
(34) Fryzuk, M. D. *Acc. Chem. Res.* **2008**, *42*, 127−133.
(35) Chirik, P. J. *Dalton Trans.* **2007**, *0*, 16−25.
(36) Hirotsu, M.; Fontaine, P. P.; Zavalij, P. Y.; Sita, L. R. *J. Am. Chem. Soc.* **2007**, *129*, 12690−12692.
(37) Davis, K. M.; Mattern, B. A.; Pacold, J. I.; Zakharova, T.; Brewe, D.; Kosheleva, I.; Henning, R. W.; Graber, T. J.; Heald, S. M.; Seidler, G. T.; Pushkar, Y. *J. Phys. Chem. Lett.* **2012**, *3*, 1858−1864.
(38) Alonso-Mori, R.; Kern, J.; Gildea, R. J.; Sokaras, D.; Weng, T.-C.; Lassalle-Kaiser, B.; Tran, R.; Hattne, J.; Laksmono, H.; Hellmich, J.; Glöckner, C.; Echols, N.; Sierra, R. G.; Schafer, D. W.; Sellberg, J.; Kenney, C.; Herbst, R.; Pines, J.; Hart, P.; Herrmann, S.; Grosse-Kunstleve, R. W.; Latimer, M. J.; Fry, A. R.; Messerschmidt, M. M.; Miahnahri, A.; Seibert, M. M.; Zwart, P. H.; White, W. E.; Adams, P. D.; Bogan, M. J.; Boutet, S.; Williams, G. J.; Zouni, A.; Messinger, J.; Glatzel, P.; Sauter, N. K.; Yachandra, V. K.; Yano, J.; Bergmann, U. *Proc. Natl. Acad. Sci.* **2012**, *109*, 19103−19107.
(39) Szlachetko, J.; Nachtegaal, M.; Boni, E. d.; Willimann, M.; Safonova, O.; Sa, J.; Smolentsev, G.; Szlachetko, M.; Bokhoven, J. A. v.; Dousse, J.-C.; Hoszowska, J.; Kayser, Y.; Jagodzinski, P.; Bergamaschi, A.; Schmitt, B.; David, C.; Lucke, A. *Rev. Sci. Instrum.* **2012**, *83*, 103105.